Motion Effects on Leading-Edge Vortex Behavior Over Delta Wings and Generalized Modeling

X.Z. Huang and E.S. Hanff
Institute for Aerospace Research
NRC Building M10, Room 208
Montreal Road
Ottawa, Ontario, K1A 0R6
Canada

ABSTRACT

Effects of static attitude and three different motions on vortex behavior and its breakdown over delta wings have been investigated. These motions include 1) harmonic oscillation or ramp-and-hold motion in roll at constant resultant angle of attack, 2) harmonic oscillation or ramp-and-hold in pitch and 3) coning at constant resultant angle of attack A basic 65° delta wing configuration was tested in two wind tunnels as well as in a water tunnel. A roll rig, pitch rig and coning rig (OPLEC) were employed for the investigation.

Quite different flow characteristics have been found within the spiral vortex breakdown region even under steady conditions. The point where vortex breaks down into large scale turbulence has a very long response time to perturbations and is the major cause for the dramatic time dependence observed in the airloads. In addition, bi-stable vortex breakdown locations are observed in the case of slender delta wings when breakdown is located close to the trailing edge. Under dynamic conditions, the behavior of the vortex and its breakdown region have been found to be highly dependent on motion waveform and reduced angular rates

An analytical model based on the Nonlinear Indicial Response Method and a formulation suggested by Tobak et al, and capable of reflecting the above effects is proposed to predict breakdown location under dynamic conditions.

SYMBOLS

b	wing span	
c_0	wing root chord	
D	vortex core diameter	
s	local semi-span	
U_∞	freestream velocity	
X_{VB}	chordwise vortex breakdown location	
x_{VB}	non-dimensional vortex breakdown location	$= \dfrac{X_{VB}}{c}$
α	angle of attack	
$\dot{\alpha}$	non-dimensional pitch rate	$= \dfrac{\omega c}{U_\infty}$
β	sideslip angle	
δ	deviation	

Report Documentation Page

Public reporting burden for the collection of information is estimated to average 1 hour per response, including the time for reviewing instructions, searching existing data sources, gathering and maintaining the data needed, and completing and reviewing the collection of information. Send comments regarding this burden estimate or any other aspect of this collection of information, including suggestions for reducing this burden, to Washington Headquarters Services, Directorate for Information Operations and Reports, 1215 Jefferson Davis Highway, Suite 1204, Arlington VA 22202-4302. Respondents should be aware that notwithstanding any other provision of law, no person shall be subject to a penalty for failing to comply with a collection of information if it does not display a currently valid OMB control number.

1. REPORT DATE	2. REPORT TYPE	3. DATES COVERED
00 MAR 2003	**N/A**	**-**

4. TITLE AND SUBTITLE		5a. CONTRACT NUMBER
Motion Effects on Leading-Edge Vortex Behavior Over Delta Wings and Generalized Modeling		5b. GRANT NUMBER
		5c. PROGRAM ELEMENT NUMBER
6. AUTHOR(S)		5d. PROJECT NUMBER
		5e. TASK NUMBER
		5f. WORK UNIT NUMBER
7. PERFORMING ORGANIZATION NAME(S) AND ADDRESS(ES)		8. PERFORMING ORGANIZATION REPORT NUMBER
NATO, Research and Technology Organisation, BP 25, 7 rue Ancelle, F-92201 Neuilly-Sur-Seine Cedex, France		
9. SPONSORING/MONITORING AGENCY NAME(S) AND ADDRESS(ES)		10. SPONSOR/MONITOR'S ACRONYM(S)
		11. SPONSOR/MONITOR'S REPORT NUMBER(S)

12. DISTRIBUTION/AVAILABILITY STATEMENT
Approved for public release, distribution unlimited

13. SUPPLEMENTARY NOTES
Also see: ADM001490, The original document contains color images.

14. ABSTRACT

15. SUBJECT TERMS

16. SECURITY CLASSIFICATION OF:			17. LIMITATION OF ABSTRACT	18. NUMBER OF PAGES	19a. NAME OF RESPONSIBLE PERSON
a. REPORT **unclassified**	b. ABSTRACT **unclassified**	c. THIS PAGE **unclassified**	**UU**	**22**	

Δ	standard deviation
Λ	leading-edge sweepback angle
σ	sting angle or resultant angle of attack
ϕ	aerodynamic roll angle
$\dot{\phi}$	non-dimensional roll rate
τ	convection time
ω	angular pitch rate
Ω	coning rate
$\overline{\Omega}$	non-dimensional coning rate

$$\dot{\phi} = \frac{\dot{\Phi}b}{2U_\infty}$$

INTRODUCTION

High-performance combat aircraft should be capable of flying at high incidence and high angular rates, where flows are usually dominated by strong wing or LEX leading-edge vortices needed to generate large aerodynamic forces. However, the behavior of these vortices and, especially, their breakdown over lifting surfaces are the major cause for the observed airload nonlinearities and time dependence in the advanced maneuvering regime. Thus, a clear understanding of the behavior of vortices and their breakdown is an essential requirement for solving the flight mechanics problems in that regime.

To date, most of the experimental dynamic studies have been limited to motions in one plane, either pitch, yaw or roll . Given that the behavior of a vortex and its breakdown are nonlinear processes, previous linear assumptions, that allow the superposition of the effects due to the motion orthogonal components is not legitimate.

In the nonlinear regime, where vortex behavior and its breakdown depend on all the motion variables and their histories, the response to motions in one plane clearly will be influenced by the presence of other motions. The practical difficulties of imparting all motions at once, induced Tobak and his colleagues to investigate this coupling in a nonlinear context[1]. They found that for nearly rectilinear flight paths in the non-linear regime, the aerodynamic response to an arbitrary motion may be obtained from the contributions from four simple motions which are all at a constant inclination of the body axes with respect to the velocity vector. These four simple motions are: 1) fixed attitude, 2) oscillation in roll at constant resultant angle of attack, 3) oscillation in pitch about a fixed resultant angle of attack and 4) coning at constant resultant angle of attack (Fig. 1).

Since the aerodynamic coefficients are functions of the flow field, which at high incidence is overwhelmingly vortex dominated, it stands to reason that a similar methodology as used by Tobak can be used as a first step in describing vortex behavior in the case of complex motions. Thus, the behavior of the vortex and its breakdown under those four simple motions are discussed in this paper.

EXPERIMENTAL SET-UP

Studies of the effects of the above motions were conducted at the IAR 6x9 ft, USAF 7x10ft wind tunnels and IAR 15x20 water tunnel respectively. A roll rig, a pitch rig[2,3] and an orbital-platform-coning (OPLEC) rig[4,5,6] were employed in the studies (Fig. 2 to Fig. 4). The roll rig is capable of imparting an harmonic motion with amplitude and frequency of up to 40° and 18 Hz respectively with a maximum roll angle offset ±50°. The pitch rig rotated the model around an axis 5.39 in. behind the trailing edge over a

range of angle of attack from –1° to 90° with minimum transition time of 75 ms. In the case of the OPLEC apparatus, the model is mounted on a sting attached to an annular platform riding on the outer surface of a stationary cylindrical test section insert. This configuration results in minimal aerodynamic interference as the strong support interference, present in conventional rigs caused by the rotating support arm, is eliminated.

The basic configuration in the investigation is a 65° delta wing (Fig. 5). Static sweeps as well as large-amplitude, high-rate harmonic and ramp and hold motions in pitch and roll, as well as coning motion were performed. The tests were conducted at a Reynolds number of 36000 and 3.6 million per foot in the water tunnel and wind tunnel respectively. In addition, some slender delta wings were tested statically in IAR water tunnel.

In the wind tunnel experiments, leading-edge vortex was visualized by seeding the flow with smoke or natural condensation and applying a laser light sheet oriented normal to the body axis thus yielding a section view of the vortex or longitudinally passing through the vortex core over most of its length. In the smoke tests, the plume of smoke was made to impinge near the nodal point of attachment on the windward side.   If the lighting set-up and gray scale sensitivity is fixed during the experiment, the gray level is approximately proportion to w/u_x. Thus, the image reflects the behavior of the rotational vortex core[7]. In order to obtain a reasonably high temporal resolution, images were captured by a high-speed video camera with a frame rate of up to 1000 fps. Video frames were individually digitized using an 8 bit gray scale (black=0, white=255). In general, an intact vortex appears as a ring of high brightness with a dark core whereas a burst vortex appears as an evenly illuminated disk with somewhat more diffuse edges. Occasionally, the darker sub-core is not discernible due to saturation of the video camera. The edge of the vortex core was assumed to be where the maximum gradient occurs. Once the edge was defined, its diameter and position relative to the model were determined. After the center of the vortex was obtained, the spanwise gray level profiles along the vortex axis were further obtained. The criteria for determining vortex breakdown in the section view is a little downstream of that based on the kink point of the vortex filament in a longitudinal view, as it is difficult to detect the kink point in the former view. In the water tunnel experiments dye is injected through two 0.008 in. diameter ports located at 5% c_0 and half local semi-span on the windward side. Two video cameras provide a top and side view of the vortices. Breakdown was defined at the kink of the vortex filament.

EXPERIMENT RESULTS

Basic behavior of vortex in steady situation

As described by Lambourne[8] a vortex exhibits three stages 1). Axial filament is almost straight up to a kink point. 2) Downstream of this point the vortex remains intact but it is deformed into a spiral that rotates in the opposite direction as the spiral streamline of the intact vortex. 3) After a few turns, the vortex eventually breaks down into large-scale turbulence. It is worthwhile to mention that in Lambourne's definition, the vortex is still intact downstream of the kink point which is different from the prevalent definition.

These three-stages were clearly seen in the experiments. Large-scale fluctuations were found in the breakdown region even under static conditions. As examples, Fig. 6

shows two typical patterns obtained for the same model and attitude. To facilitate descriptions, the vortex filament kink is denoted as point A in Fig. 5 while the subsequent turbulent breakdown is denoted as point B. Two white spots marked on the wing surface are employed as reference for measuring distances. The distance between the two marks is 0.34 root chord, c_0. Interestingly, the breakdown process can cover almost 0.3 c_0 as seen from Fig. 6. More importantly, the behavior of the two points are quite distinct. Whereas the locations of point B are nearly the same in both cases, those of point A are radically different.

The high level of unsteadiness in the breakdown region is illustrated in Fig. 7 where selected pairs of consecutive frames are shown. The frames in the first and second pairs are separated by 4 ms while the frames in the last pair are taken 1 ms apart, corresponding to 0.60 and 0.15 convection times, c/U_∞, respectively. These typical figures show that the length of the spiral breakdown region can change significantly within a convection time indicating that the propagation speed of point A can approach $0.5U_\infty \cos\alpha$ whereas the very small displacement of point B reflects its much lower propagation speed. Furthermore, Fig. 7 seems to suggest that for a given angle of attack when the instantaneous flow condition promotes vortex breakdown, point A moves rapidly forward while the response of point B is extremely sluggish, resulting in an increase of the helix angle, a reduction in the spiral diameter with the pitch remaining more or less constant. On the other hand when the instantaneous flow condition delays breakdown, point A moves rapidly downstream with point B again responding very slowly, resulting in a decrease of the helix angle and an increase in the spiral diameter, with pitch again remaining more or less constant. The length of the breakdown region therefore changes mainly as a result of changes in the number of spiral turns contained therein. The additional loops needed to lengthen the breakdown region seem to be generated by curling up of the previously intact vortex just forward of point A. Likewise a straightening of the upstream turns within the breakdown region seems to cause its shortening.

Energy in the spiral breakdown region decays gradually between points A and B resulting in a slower streamwise reduction in suction than in the case of bubble breakdown. Moreover, the much slower response of point B clearly dictates the very important time lags observed in the breakdown motion reflected by the movement of Point suggesting that Point B is a more important characteristic parameter than Point A.

Furthermore, it has been found that the breakdown unsteady behavior is significantly affected by geometric discontinuities on the model surface possibly through their effect on the local streamwise pressure gradient. Significantly larger fluctuations of the breakdown location were observed when breakdown occurred over the leading- and trailing-edge bevels as demonstrated by the standard and maximum deviations plotted in Fig.8. This result was obtained in a water tunnel for a 65° delta wing with a 10° leading- and trailing edge bevels. In order to assess the stability of the breakdown process, experiments were conducted in which an obstruction was momentarily introduced as a pulse input at a location aft of breakdown for a 75° delta wing at α=36°, 34° and 31.95° corresponding to x_{VB}/c= 0.51, 0.67 and 0.94 respectively. In the first two cases, the pulse input resulted in a momentary forward displacement of the breakdown location which quickly returned to its original position once the obstruction was removed as depicted in Fig. 9 and Fig. 10. The breakdown location on the other wing half exhibited the opposite

behavior but also returned to its original position after removing the disturbance. Similar responses were obtained for wings with a smaller sweepback angle.

In the case where breakdown was in the vicinity of the trailing edge at α=31.95°, however, a totally different phenomenon was observed. Breakdown initially occurred symmetrically at $x_{VB} \approx 0.94$; and if the obstruction was applied sufficiently aft of breakdown, the response was analogous to those at higher angles of attack. However, after introducing and withdrawing the obstruction closer to the breakdown location, the breakdown location unexpectedly moved forward to a stable position 5% upstream of the initial symmetric location. In the meantime the breakdown point of the other vortex commenced a gradual motion that would place it well aft of the trailing edge, taking over hundred free-stream convection times to reach a stable position at $x_{VB} \approx 1.4$. Application of the disturbance aft of the latter could either lead to a reversal of the situation or a symmetric arrangement. An edited time history of the breakdown locations, where long waiting times have been removed for clarity, is shown in Fig. 11.

The various breakdown responses to the above phenomena can be readily discerned, which means that more than one stable location exists for the time-averaged breakdown point. The attractor associated with the symmetric arrangement was smaller than that for the asymmetric ones if the breakdown location is close to the trailing edge. It is, however, worthwhile to mention that this phenomenon is only observed over more slender wing with breakdown location near the trailing edge.

Motion effect on vortex behavior and its breakdown

Under dynamic conditions, the behavior of the leading-edge vortex is considerably more complex due to the motion effects which are superimposed to the steady ones. Fig. 12 shows the non-dimensional vortex diameter vs. roll angle over the right wing half at several stations for different rolling oscillation frequencies. These results were obtained from gray level analysis of the vortex section view. The static results, based on the average value over the intact vortex are also included for comparison. Each dynamic trajectory has two branches, the left and right ones corresponding to the upstroke and downstroke respectively. The first point on the left branch and the last one on the right branch correspond to the formation and breakdown of the vortex at the indicated stations. For a given roll angle, the dynamic D/s is larger than the corresponding static value during the upstroke, while it is smaller during the downstroke. The difference between the dynamic and static values increases with amplitude and frequency, although at higher angular rates this process tends to saturate.

There is abundant evidence that the motion of leading-edge vortex breakdown plays an important role in creating the airload non-linearities and time dependence observed under dynamic conditions. Considerable effort has, therefore, been directed at observing the movement of breakdown location. which must be done by means of an averaging process to eliminate the above fluctuations a process which is greatly simplified by using point B because of its inherent slow response

The effect of rolling oscillation frequency on breakdown motion over the right wing half is shown in Fig. 13. The response to the rolling oscillation exhibits a hysteretic behavior even at very low reduced frequencies and becomes more pronounced at higher frequencies. The differences between the results at k=0.14 and k=0.2 are relatively small due to the saturation process alluded to above. The longitudinal range traversed by the

breakdown point decreases at higher frequencies due to its limited propagation speed, which has been found to be approximately 0.1 U_∞ and 0.2 U_∞ in the forward and aft directions respectively. Sections of the loops are not shown due to insufficient frames to reliably establish the breakdown location. The effect of amplitude is shown in Fig. 14. In this case the loop tends to expand rather evenly with amplitude without exhibiting saturation, suggesting a more linear effect than that of frequency.

Under transient ramp-and-hold rolling conditions, significant time lags are similarly present with respect to their corresponding time-averaged static locations. As examples, the instantaneous vortex breakdown location measured during ramp-and-hold from +16° to -16° roll angle or reversed from -16° to +16° motion with different ramp rates are depicted in Fig. 15. The breakdown location shifts more as the ramp rate increases. For example, the average breakdown location was delayed by 1° roll angle at the rate of ±0.00072, while it was delayed 4° at the roll rate of ±0.0028.

The effect of pitch motion on vortex behavior can be observed from Fig. 16 to Fig. 18. As an illustration, the time-averaged position for the case of pitch-down transition from α=30° to 20° are depicted in Fig. 16a where the static ones are superimposed for comparison. Initially, breakdown is at its static location and moves aft when the angle of attack decreases. However, in spite of the small non-dimensional angular rate, the instantaneous breakdown location rapidly falls behind its static counterpart. Examples of the effect of pitch-up motion between α=20° and 50° at different angular rates are shown in Fig. 17a and Fig. 17b. In both cases breakdown is located aft of the trailing edge at the motion onset and move on to the wing at a larger angle of attack dependent on the angular rate. Interestingly, at the lower rate the instantaneous breakdown location tends to approach its static value (Fig. 17a), while the angular rate is still increasing. Results corresponding to the same motion but at a higher angular rate, show that breakdown reaches the trailing edge at an even higher angle of attack (α=31°) far later than that under static conditions.

In addition, pitch motion also causes axial compression and expansion of the breakdown region between points A and B. As seen in Fig. 16 point A tends to "catch up" point B due to its higher speed of response during pitch-down while the distance seems to grow reaching a maximum value at $\alpha \approx$31° during pitch-up (Fig. 17). This breakdown behavior, together with the previously described unsteady one, appears to suggest that although point A tends to react much faster than B, the latter in some way restricts the motion of the former.

Fluctuations caused by flow unsteadiness are also observed under dynamic conditions. Fig. 18, as an example, shows two consecutive images taken at instantaneous angles of attack α=24.43° and α=24.40° during a pitch down motion. The time difference is 1 ms. Point A in Fig. 18b should move aft compared with that in Fig. 17, instead, it moves significantly forward. In the meantime there is no significant change in point B consistent with the previously described sluggishness of the point B response.

Coning motion effects on the leading-edge vortices and their breakdown are illustrated in Fig. 19. As examples, the measured breakdown locations for different coning rates and resultant angles of attack are depicted in Fig. 20. Generally speaking, the coning motion promotes breakdown on the advancing side of the wing while delaying it on the receding side (based on the part of the model forward of the intersection with

coning axis). The coning motion also affects the trajectory of the vortex core by causing it to acquire a gentle spiral shape. A positive coning rate (clockwise in back view) displaces the trajectory of the port vortex core outboard on the forward portion and inboard in the aft portion of the wing half.

GENERALIZED MODELING OF MOTIONS' EFFECTS

So far vortex behavior under four different motions have been studied on models with the same geometry. In order to predict vortex behavior due to an arbitrary motion in the nonlinear regime a generalized model based on Tobak's Nonlinear Indicial Response method is proposed. Such an approach becomes necessary because in this regime there are couplings between the effects of the motion orthogonal components and moreover, these effects are also dependent on the motion history. Obviously the linear model which assumes that the indicial responses are independent of motion history and allows the superposition of independent effects due to the orthogonal motion components is not applicable under these conditions.

Thus Tobak's approach, originally developed to predict airloads is adopted and extended to a general variable representing the flow field or more specifically the vortex breakdown location- at high angle of attack and high angular rate. This appears to be legitimate as aerodynamic coefficients reflect the integrated effect of the flow field which at high incidence is clearly vortex dominated. Moreover, experimental results have demonstrated that the vortex turbulent breakdown location (point B) is less affected by flow unsteadiness and is thus considered to be the variable of interest, which as a first approximation may be taken as a continuous function of the motion variables except in the cases discussed above of highly swept delta wings when breakdown is near the trailing edge, or the model leeward surface exhibits geometric discontinuities. Given the dominant effect of breakdown on aerodynamic loads, if its movement is solved it can be taken as an internal variable towards the final estimation of aerodynamic loads in the nonlinear regime. Preliminary studies conducted in 1992 and later in 2000 show prospective results which agree with the experimental results[9,10]. A similar idea but using a different approach was proposed by Goman and Khrabrov[11]

According to this method, the aerodynamic response (breakdown location in this case) can be built up from the responses to a limited number of well-defined characteristic motions. In general, x_{VB} can be expressed as a functional of $\sigma(\xi)$, $\phi(\xi)$ and $\Omega(\xi)$, in an arbitrary motion over the interval $-\infty < \xi < t$:

$$x_{VB}(t) = x_{VB}[\sigma(\xi), \phi(\xi), \Omega(\xi)] \tag{1a}$$

or explicitly in the form of an indicial response functional

$$x_{VB}(t) = x_{VB}[\sigma(\xi), \phi(\xi), \Omega(\xi); t, \tau] \tag{1b}$$

which means that $x_{VB}(t)$ is both a functional of $\sigma(\xi), \phi(\xi), \Omega(\xi)$ and a function of t and τ. If the functional is Frechét differentiable over $(\sigma(\xi), \phi(\xi), \Omega(\xi))$ for the motion at hand, the following expression applies:

$$f'(\sigma, \phi, \Omega) = f_\sigma(\sigma, \phi, \Omega)\Delta\sigma + f_\phi(\sigma, \phi, \Omega)\Delta\phi + f_\Omega(\sigma, \phi, \Omega)\Delta\Omega \tag{2}$$

where *f* stands for x_{VB} in this case and $\Delta\sigma$, $\Delta\phi$, $\Delta\Omega$ are unit step changes in σ, ϕ, Ω, respectively.

Based on the NIR methods (Eqn (19) in Ref. 1), the vortex breakdown location can then be given by

$$x_{VB}(t) = x_{VB0}(0) + \int_0^t x_{VB1}[\sigma(\xi), \phi(\xi), \Omega(\xi); t, \tau]\frac{d\sigma(\tau)}{d\tau}d\tau + \int_0^t x_{VB2}[\sigma(\xi), \phi(\xi), \Omega(\xi); t, \tau]\frac{d\phi(\tau)}{d\tau}d\tau$$

$$+ \int_0^t x_{VB3}[\sigma(\xi), \phi(\xi), \Omega(\xi); t, \tau]\frac{d\Omega(\tau)}{d\tau}d\tau \tag{3}$$

where x_{VB1}., x_{VB2}, x_{VB3} are the indicial responses to step changes in σ, ϕ, Ω respectively. Contrary to the linear case, here the response to each step depends on the motion history prior to the step and therefore is a nonlinear function. This superposition is valid even though the system is nonlinear if the equilibrium flow at each step onset is asymptotically stable to small perturbations.

These response functions could be further understood as nonlinear responses to instantaneous angular rate in a certain period of motion history. Heuristically, the effects of angular rates can be visualized by a continuously deforming wing geometry whose surface slopes match the effective local "angles of attack", "sweepback angle", etc., induced by the angular rates.

Thus the modeling problem can be reduced to two steps: firstly, the determination of the equivalent geometric changes due to angular rates in order to establish the quasi-steady breakdown response and secondly, the determination of the unsteady response to these changes including motion history effects. The first step is relatively simple and helps to understand some of the experimental results. The second one is far more complex and has so far been successfully completed for the rolling motion case.

In the pitching case the equivalent normal surface coordinates can be found from the normal velocity distribution to be (Fig. 21a).

$$z(t) = \frac{1}{2}\frac{\dot{\alpha}(t)}{U_\infty}x^2 \tag{4}$$

In the case of rolling motion, the surface normal coordinates are obtained by simulating the roll-rate-induced chordwise angle and section angle normal to the leading-edge, and for zero roll angle are given by [8]:

$$z(t) = \frac{\dot{\phi}(t)y}{\cos\sigma(t)}[(-cor2\Lambda(t) + \frac{1}{\sin 2\Lambda(t)(1\pm\tan\sigma(t)\sin\phi(t)\tan\Lambda(t)})|y| - x] \tag{5}$$

where $\pm$ sign correspond to the right and left wing halves respectively. It is interesting to note that for $\phi=0$ the wing surface is anti-symmetrical about the body axis of x and is characterized by straight leading edges as illustrated in Fig. 21b.

Finally, in then coning motion, the lateral velocity component, U_y, induced by the coning can be estimated by means of the following kinematic equation:

$$U_y(x) = U_\infty\sin\sigma(t)\sin\phi(t) + \Omega(t)x\sin\sigma(t)\cos\varphi(t) = U_\infty\sin\sigma(t)(\sin\varphi(t) + 2\overline{\Omega}(t)(x/b)\cos\varphi(t))$$

where the chordwise coordinate x has its origin at the coning center. This additional velocity component results in changes in effective sideslip angle and additional leading-edge sweep angle:

$$\beta(x) = \sin^{-1}[U_y(x)/U_\infty] = \sin^{-1}[\sin\sigma(t)(\sin\phi(t) + 2\overline{\Omega}(t)(x/b)\cos\phi(t))] \tag{6a}$$

$$\Delta\Lambda(x) = \tan^{-1}(U_y / U_x) = \tan^{-1}[\tan\sigma(t)(\sin\phi(t) + 2\overline{\Omega}(t)(x/b)\cos\phi(t))] \qquad (6b)$$

For positive coning, the lateral velocity component and sideslip angle is negative in the forward portion and positive in the aft portion as seen in Fig. 21c.

Moreover, the local aerodynamic roll angle, ϕ_a, is also affected as follows:

$$\phi_a(x) = \tan^{-1}(U_y / U_z)$$
$$= \tan^{-1}\{[\tan\phi(t) + 2\overline{\Omega}(t)(x/b)]/[1 - 2\overline{\Omega}(t)(x/b)\tan\phi(t)]\} \qquad (6c)$$

where

$$U_z = U_\infty \sin\sigma(t)(\cos\phi(t) - 2\overline{\Omega}(t)(x/b)\sin\phi(t))$$

From a Lagrangian viewpoint the wing has different camber on each side as shown in Fig. 21d. At $\phi(t)=0$ the normal coordinates of the equivalent surface is very simple and is given by

$$z = 2\overline{\Omega}\frac{xy}{b}$$

All those changes in effective leading-edge, camber, especially in the forward portion, affect the movement of the vortex breakdown.

Other than the breakdown location, coning motion also affects the trajectory of the vortex core. When the wing is coning, the vortex core exhibits a spiral pattern as seen in Fig. 22b and 22c . Since coning introduces a lateral velocity component as seen in Fig. 21c, this lateral velocity component will push or pull the vortex core spanwise according to the direction of the lateral velocity. Thus, for example, in the positive coning rate the trajectory of vortex core moves outboard on the forward potion of receding wing half while it moves inboard on the aft. This movement will largely affect the rolling moment.

Given the extreme complexity of obtaining the previously mentioned unsteady breakdown response, experiments utilizing models deformed according to the above criteria can be conducted in order to facilitate the process.

As an example, this approach has been successfully used in the case of rolling motion yielding the following expression.[8]:

$$x_{VB}(t) = X_s(\phi(t)) + \int_{t-T}^{t} X_d(t-\tau)\dot{\phi}(\tau)d\tau \qquad (7)$$

The first term represents the effect of steady-state at time t while the second one is dynamic effect including quasi-steady and unsteady effect. The later can be explicitly expended as the summation of quasi-static and motion history effects.

$$x_{VB}(t) = X_s(\phi(t)) + X_q(\dot{\phi}(t)) \cdot X_s(\phi(t)) + \int_{t-T}^{t} X_u(t-\tau)\dot{\phi}(\tau)d\tau \qquad (8)$$

Through quasi-steady experiment[12] with deformed wing, roll rate induced quasi-steady effect is found as shown in Fig. 23. The corresponding expression is:

$$X_q(\dot{\phi}(t), \alpha) = k_q\dot{\phi}(t) = \frac{0.91}{\tan\alpha(t)}\dot{\phi}(t) \qquad (9)$$

From experimental results, a simplified response function is obtained:

$$X_u(\phi; t, \tau, \sigma(t), \Omega(t)) = \frac{1.65}{\tan\alpha(t)}\sin\frac{\pi\tau}{T^*} \qquad (10)$$

Fig. 24 shows the good comparisons between measured and predicted breakdown locations. Similar procedures can in principle be applied to pitch and coning motions. When all those unknown in Eqn. (3) are solved, the movements of vortex breakdown location under arbitrary motion could then be obtained.

ACKNOWLEDGEMENTS

REFERENCES

1. Tobak, M. and Schiff, L.B., "Aerodynamic Mathematical Modeling – Basic Concepts," AGARD LS-114, Paper 1, March 1981.
2. Hanff, E.S., Kapoor, K. Anstey, C.R. and Prini, A., "Large-Amplitude High-Rate Oscillation System for the measurement of Non-Linear Airloads," AIAA Paper 90-1426, June 1990.
3. Hanff, E.S. and Huang, X.Z., "Highlights of the IAR/WL High-Alpha Joint Program," NPU/AIAA/AFM Conference, 1996.
4. Beyers, M.E. and Huang, X.Z., "The Orbital-Platform Concept for Nonplanar Dynamic Testing", National Research Council Canada, NAE-AN-52, May 1988.
5. Cai, H.J. and Beyers, M.E., "OPLEC Rotary Experiments on the F/A-18", NRC IAR LTR-A-021, March 1998.
6. Cai, H.J. and Beyers, M.E., "OPLEC Rotary Flow Visualization Study of F/A-18 at Zero Sideslip", NRC IAR LTR-A-042, August 1999.
7. Huang, X.Z. and Hanff, E.S. "Gray Level Analysis of Off-Surface Visualization on a 65° Delta Wing Oscillating in Roll," 8th International Symposium Flow Visualization, 1998.
8. Lambourne, N.C., "The Breakdown of Certain Types of Vortex," NPL AERO REPORT 1166, 1965.
9. Huang, X.Z and Hanff, E.S., "Prediction of Leading-Edge Vortex Breakdown on a Delta Wing Oscillating in Roll," AIAA Paper 92-2677, 1992.
10. Huang, X.Z, Lou, H.Y. and Hanff, E.S., "Airload Predictions for Delta Wings at High Incidence," 22nd ICAS, 221.1, August 2000.
11. Goman, M.G. and Khrabrov,A.N., "State-Space Representation of Aerodynamic Characteristics of an Aircraft at High Angles of Attack", J. Aircraft, Vol. 31, No. 5, Sept-Oct. 1994, pp.1109-1115
12. Huang, X.Z and Hanff, E.S., "Roll Rate Induced Camber Effect on Delta Wing Leading-dge Vortex Breakdown," AIAA Paper 95-1793, 1995.
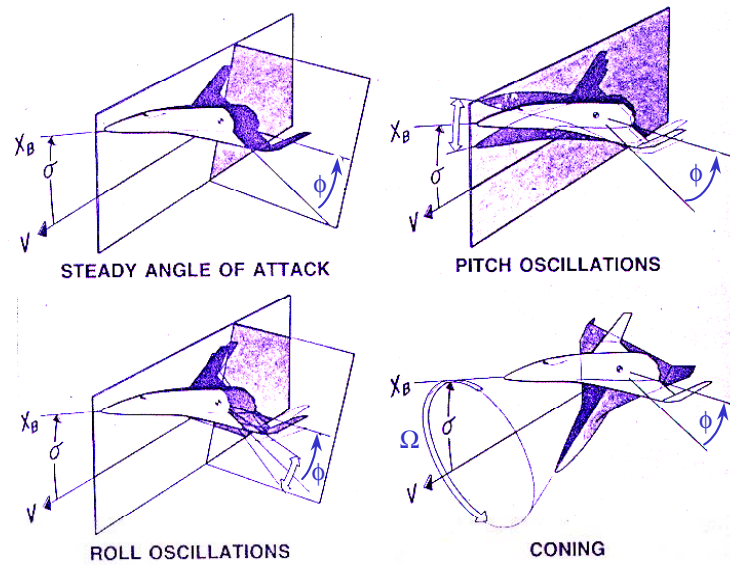
Fig. 1   Characteristic motions in the aerodynamic axis system
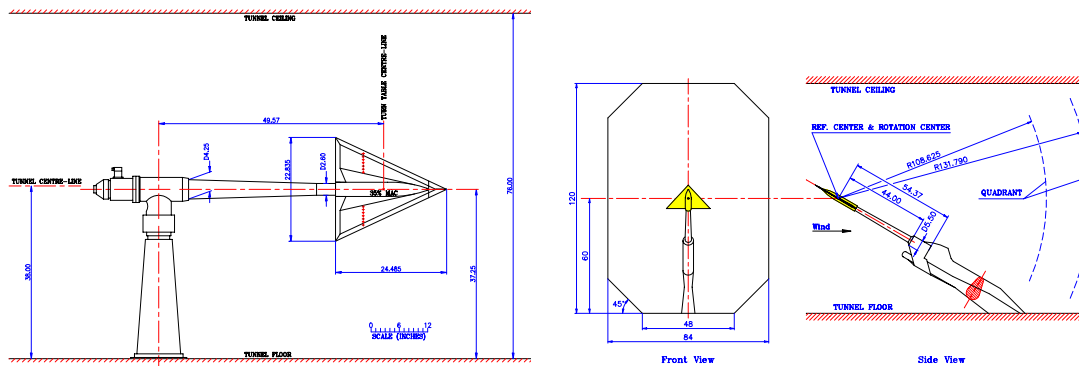
Fig. 2 Roll rig installed in IAR 6x9 ft and AFRL 7x10 ft wind tunnels
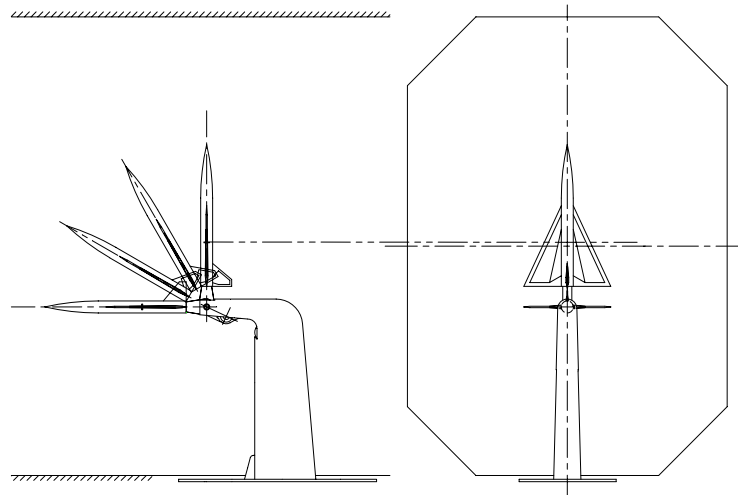
Fig. 3 Pitch rig and its installation in USAF 7x10 ft wind tunnel
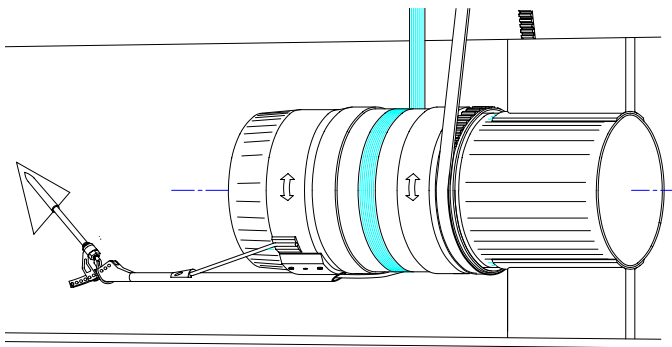
Fig. 4   Schematic layout of orbital platform apparatus
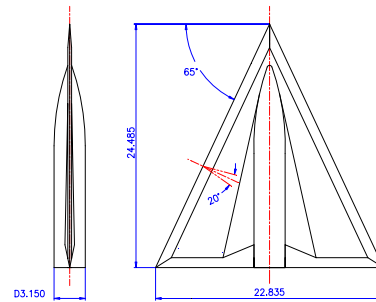
Fig. 5   65° delta wing model
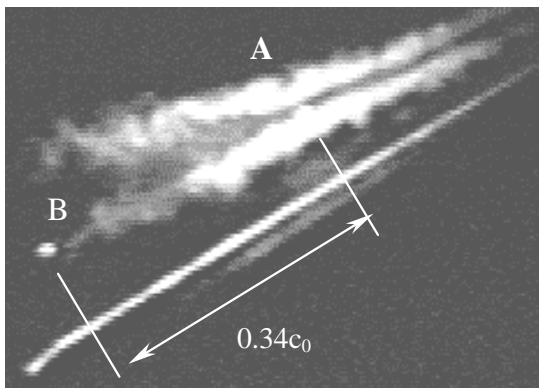
6a   slow dissipation
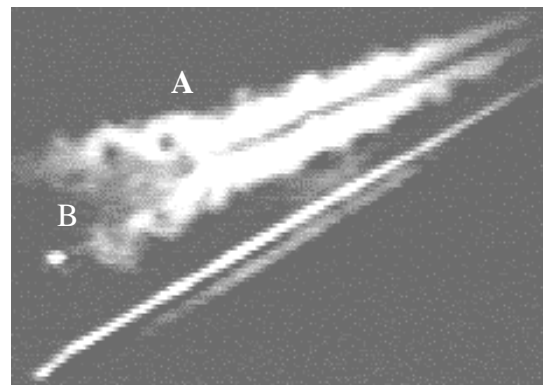
6b   fast dissipation

Fig. 6 Different spiral breakdown appearances
($\Lambda=65°$, $\alpha=26°$, $\phi=0°$)

α=26°, Δt=4 ms (0.60τ)

α=26°, Δt=4 ms (0.60τ)

α=25.5°, Δt=1 ms (0.15τ)
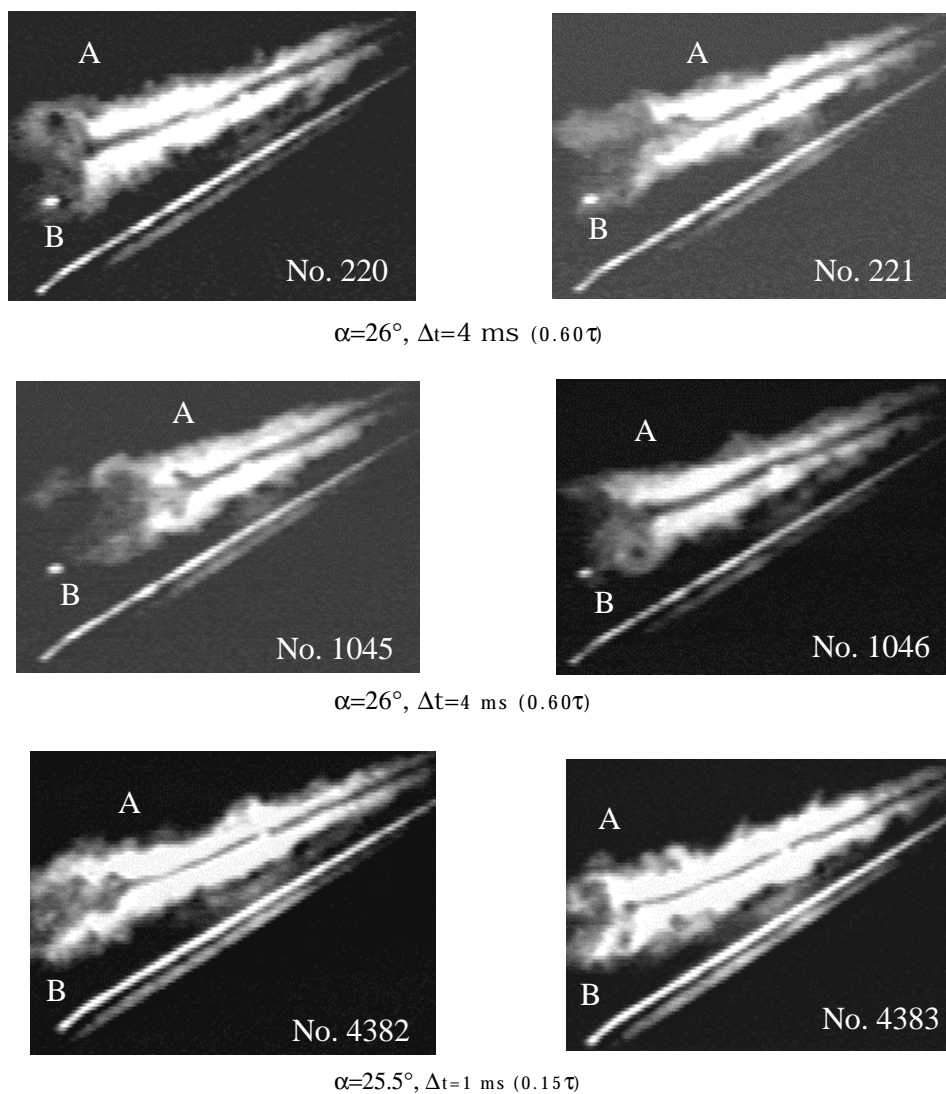
Fig. 7   Pairs of vortex breakdown images
(Λ=65°, α=26°, φ=0°)
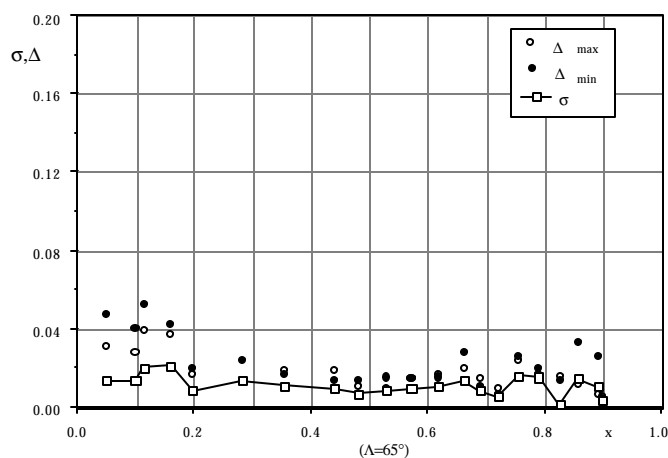
Fig. 8 Effect of leading-edge and trailing edge bevel on the scatter
of measured breakdown location
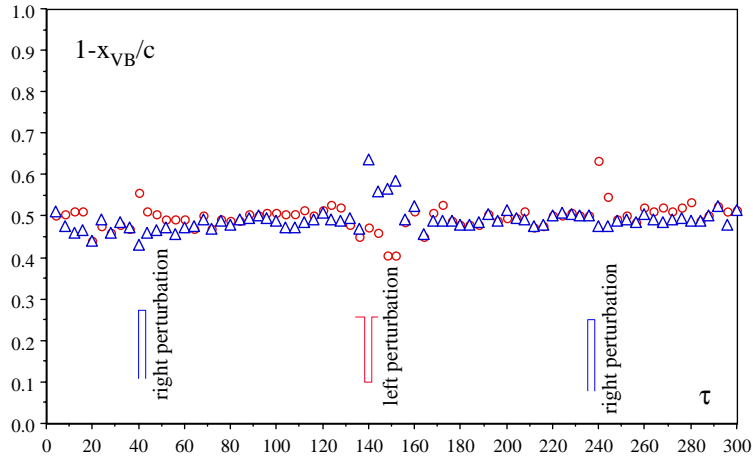
Fig. 9 Response of vortex breakdown location to perturbations (α=36°)
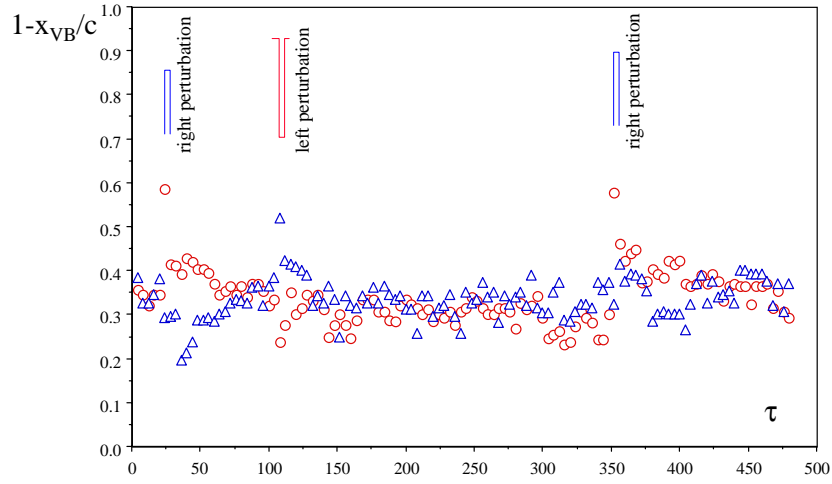
Fig. 10 Response of vortex breakdown location to perturbations (α=34°)
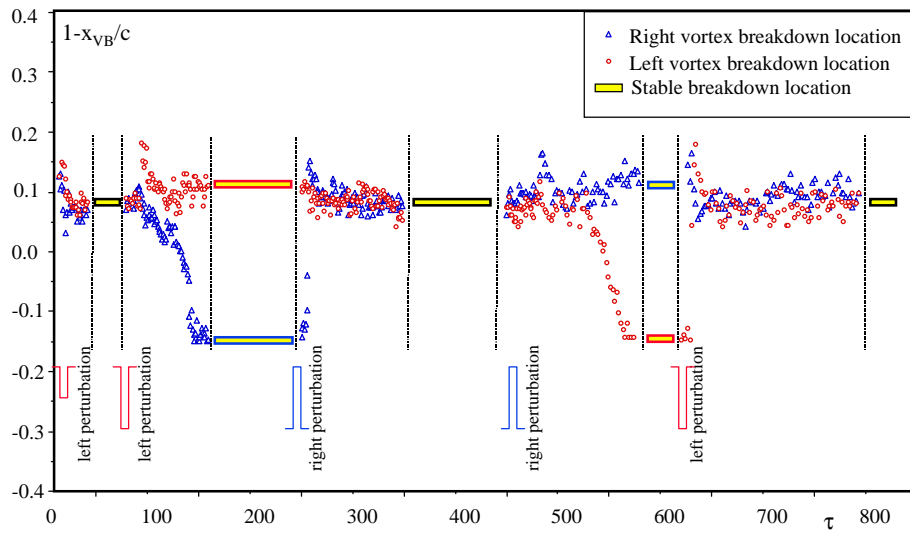
Fig. 11   Bifurcation of vortex breakdown locations
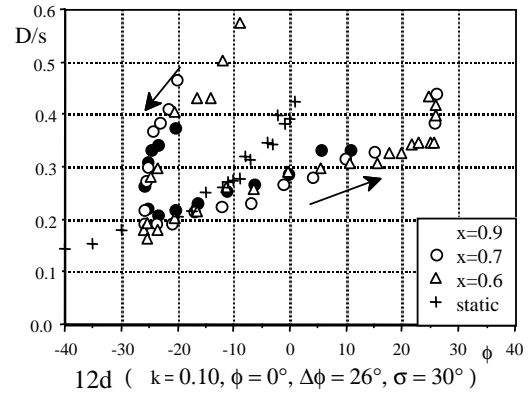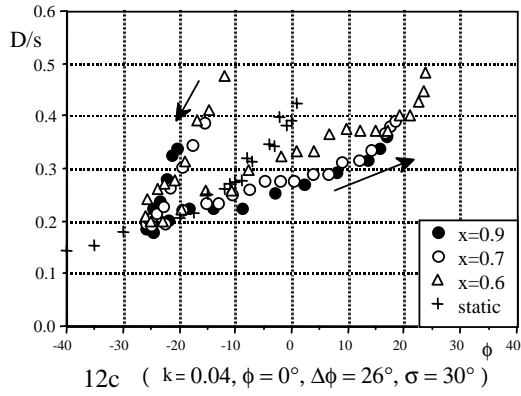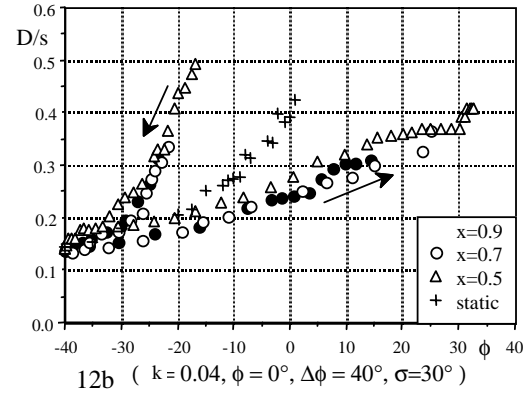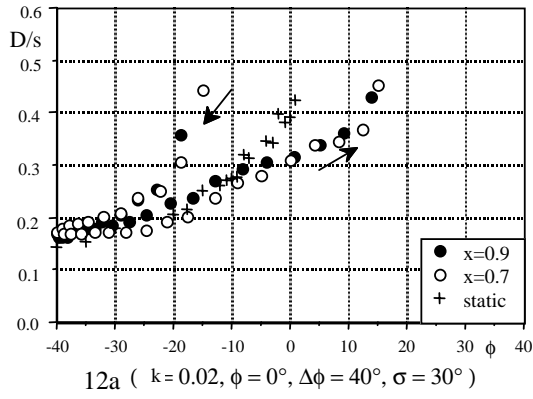
Fig. 12 Rotational vortex core diameter under rolling oscillation condition

12a　(k = 0.02, φ = 0°, Δφ = 40°, σ = 30°)

12b　(k = 0.04, φ = 0°, Δφ = 40°, σ=30°)

12c　(k = 0.04, φ = 0°, Δφ = 26°, σ = 30°)

12d　(k = 0.10, φ = 0°, Δφ = 26°, σ = 30°)

13a (σ=30°, Δφ=33°, k =0.02)

13b (σ=30°, Δφ=33°, k =0.04)

13c (σ=30°, Δφ=33°, k =0.14)

13d (σ=30°, Δφ=33°, k =0.20)
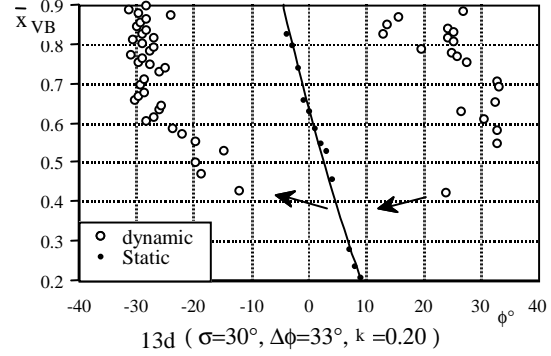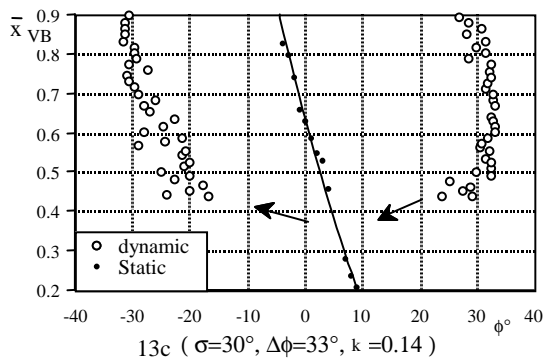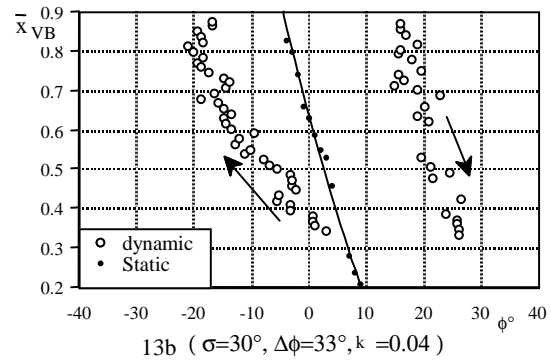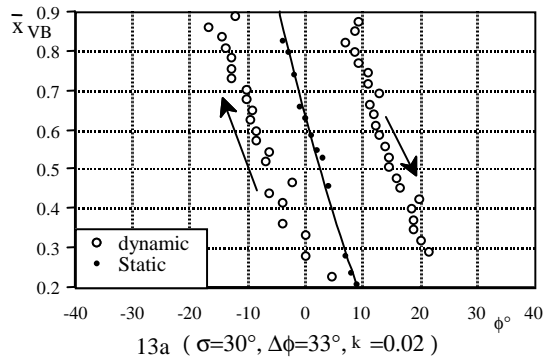
Fig. 13 Rolling frequency effect on vortex breakdown

14a (σ=30°, Δφ=19°, k =0.14)

14b (σ=30°, Δφ=26°, k =0.14)

14c (σ=30°, Δφ=33°, k =0.14)

14d (σ=30°, Δφ=40°, k =0.14)
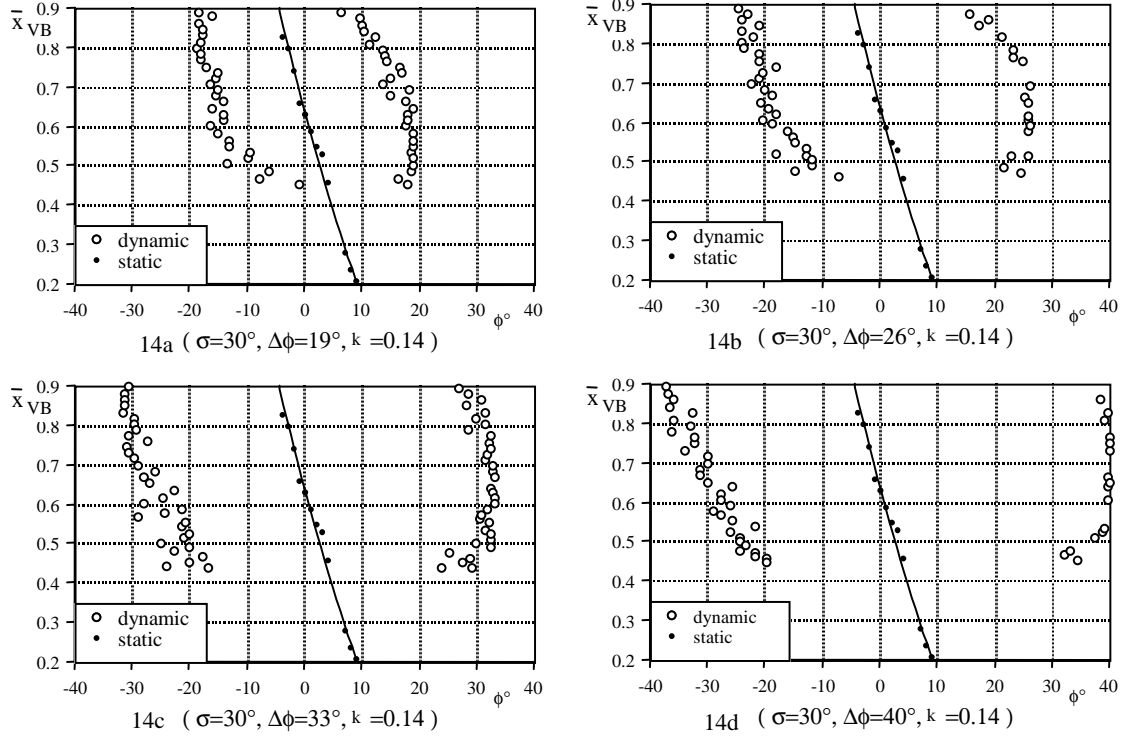
Fig. 14 Rolling amplitude effect on vortex breakdown

$\dot{\phi}$ =0.00072

$\dot{\phi}$ =-0.00072

$\dot{\phi}$ =0.0014

$\dot{\phi}$ =−0.0014
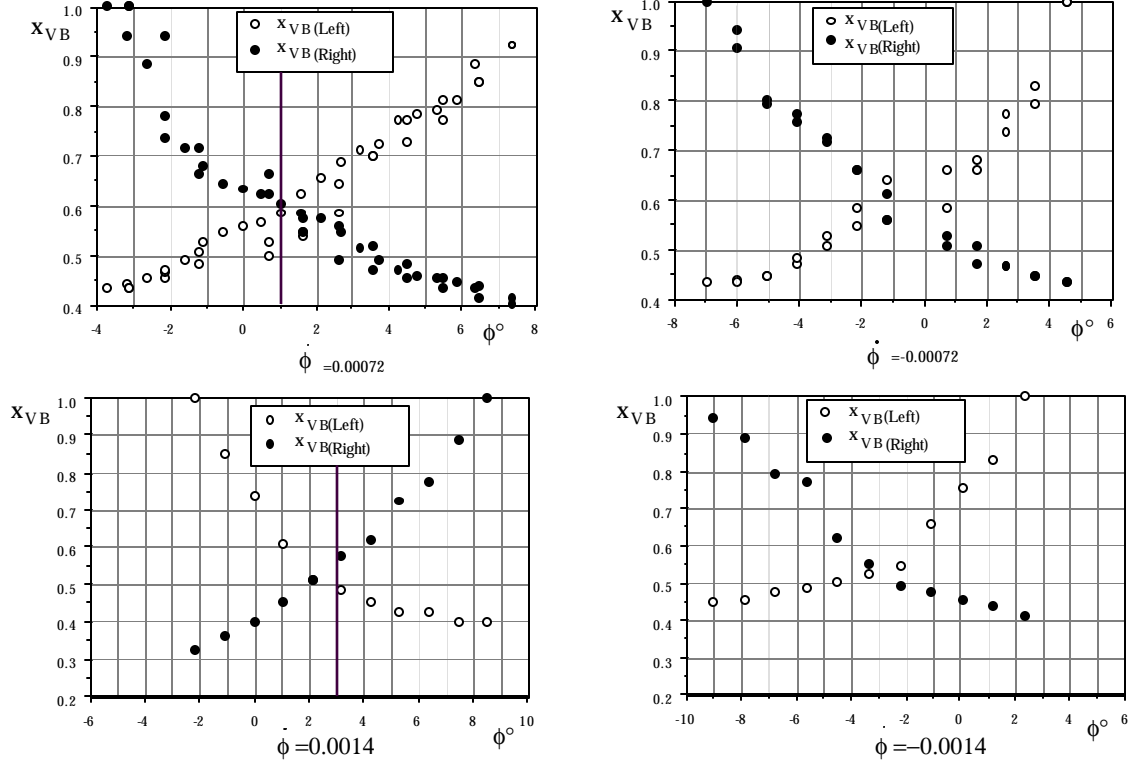
Fig. 15 Measured vortex breakdown location during ramp-and-hold motion in roll
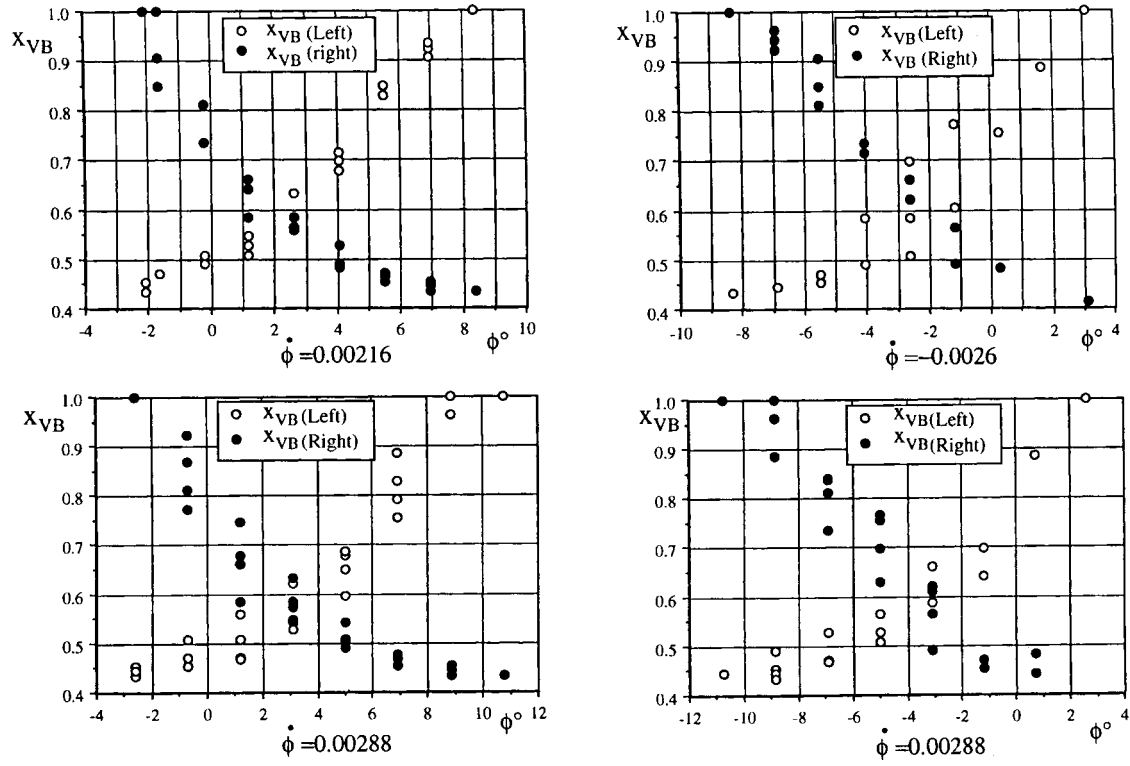
Fig. 15(Cont.) Measured vortex breakdown location during ramp-and-hold motion in roll

16a vortex breakdown movements

16b motion phase plane
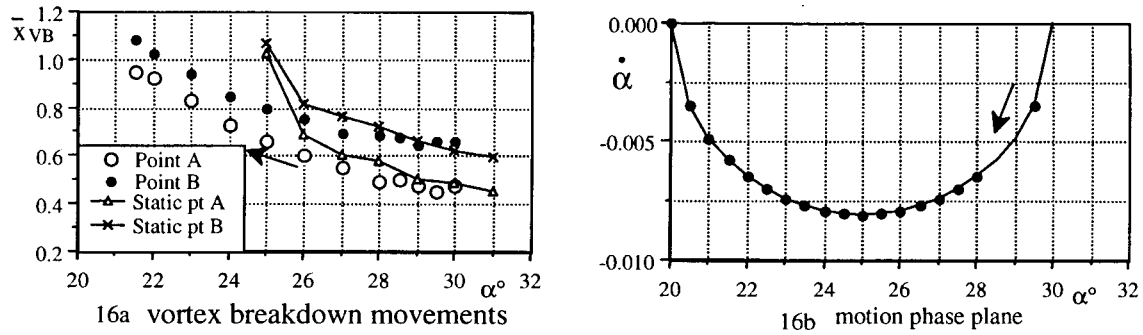
Fig. 16 Breakdown movement during pitch-down (α:30°→20°)

17a ($\dot{\alpha}_{max}$ =0.0038)

17b ($\dot{\alpha}_{max}$ =0.011)
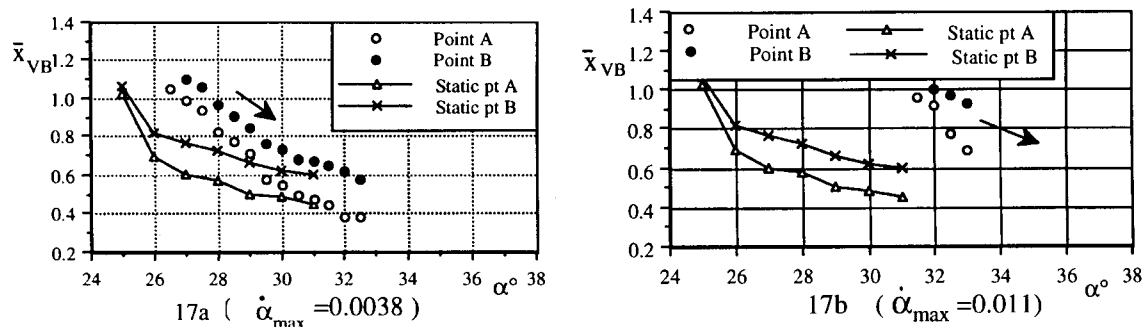
Fig. 17 Breakdown movement during pitch-up with different rates (α:20°→50°)

18a. α=24.43°
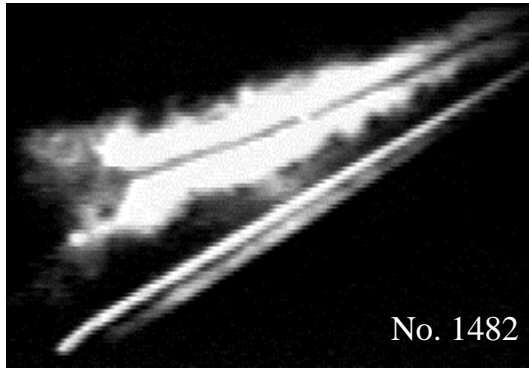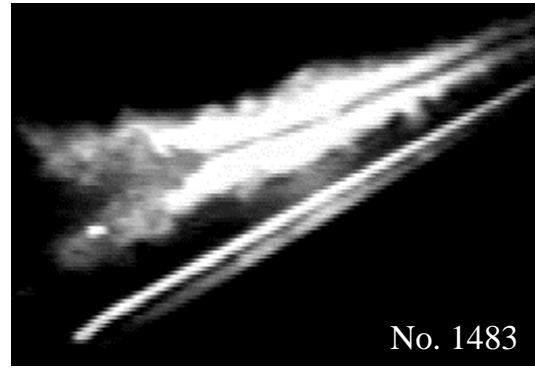
18b. α=24.40°

Fig. 18 Breakdown fluctuation during pitch-down motion (α:50°→0°)

$\overline{\Omega}$=0.51, α=37.5°, φ=2.5°
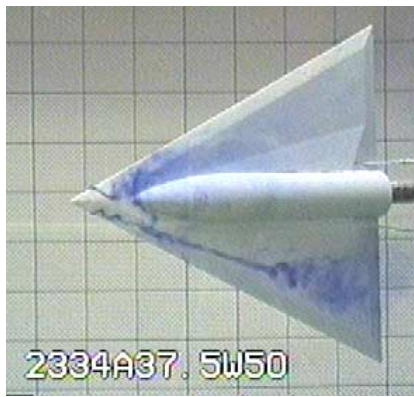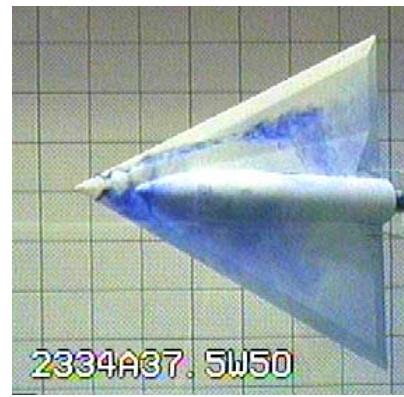
$\overline{\Omega}$=-0.51, α=37.5°, φ=2.5°

Fig. 19 flow visualization about coning effect on vortex breakdown
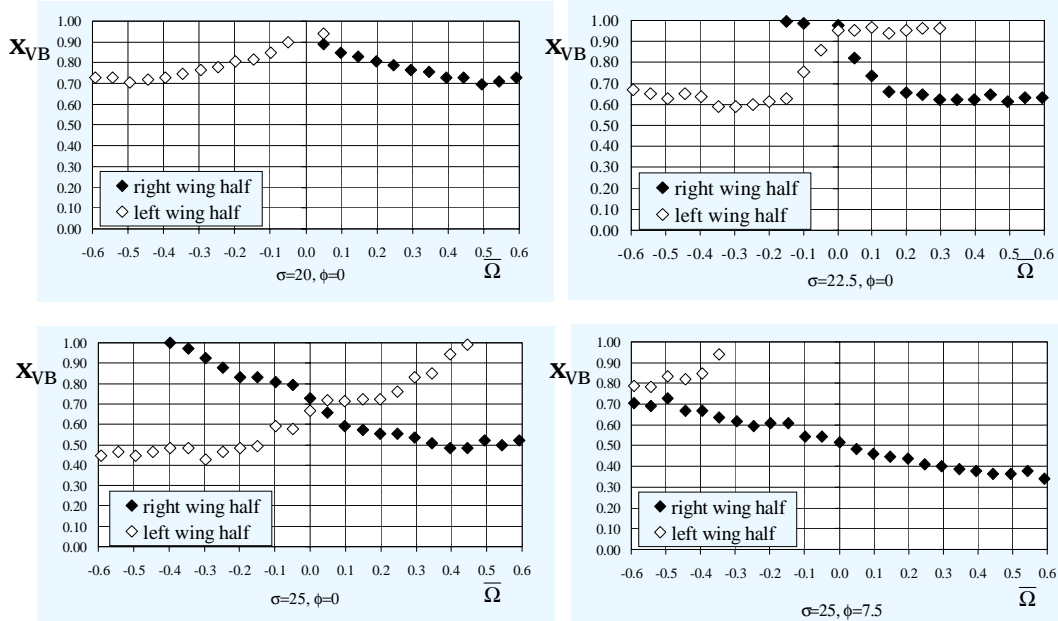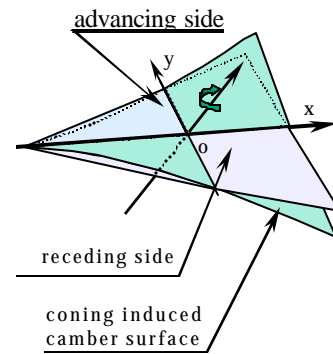

Fig. 20 Coning motion effect on vortex breakdown movement
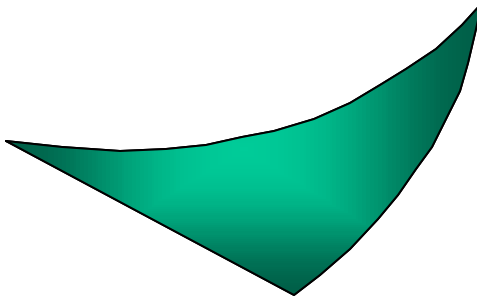
21a pitching-rate-induced camber
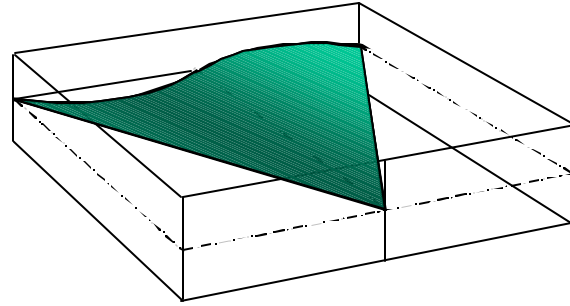
21b roll-rate-induced camber
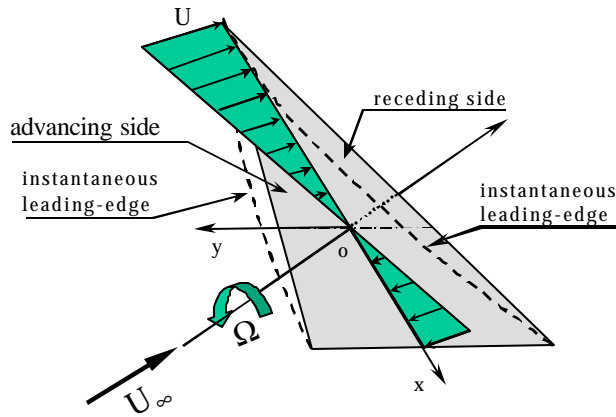
21c coning induced leading-edge shape

21d coning induced camber surface

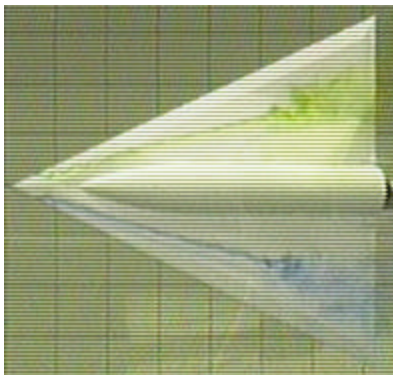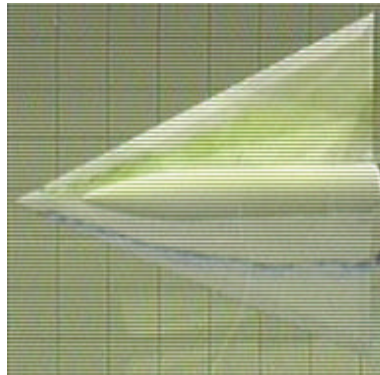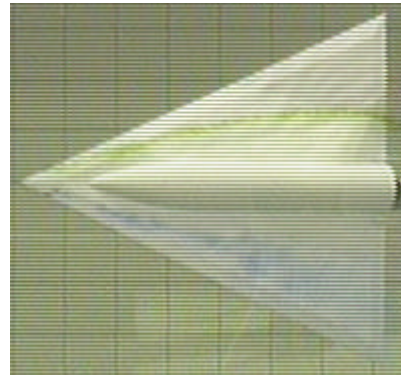Fig. 21 Motion induced kinematic changes in wing geometry

22a $\overline{\Omega}$=0, α=25°, ϕ=0°

22b $\overline{\Omega}$=0.62, α=25°, ϕ=0°

22c $\overline{\Omega}$=-0.62, α=25°, ϕ=0°

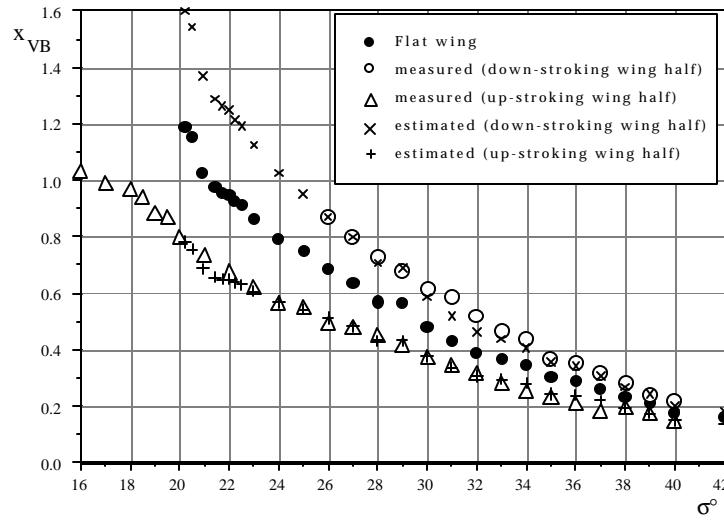Fig. 22 Leading-edge vortex trajectory under non-planar motion

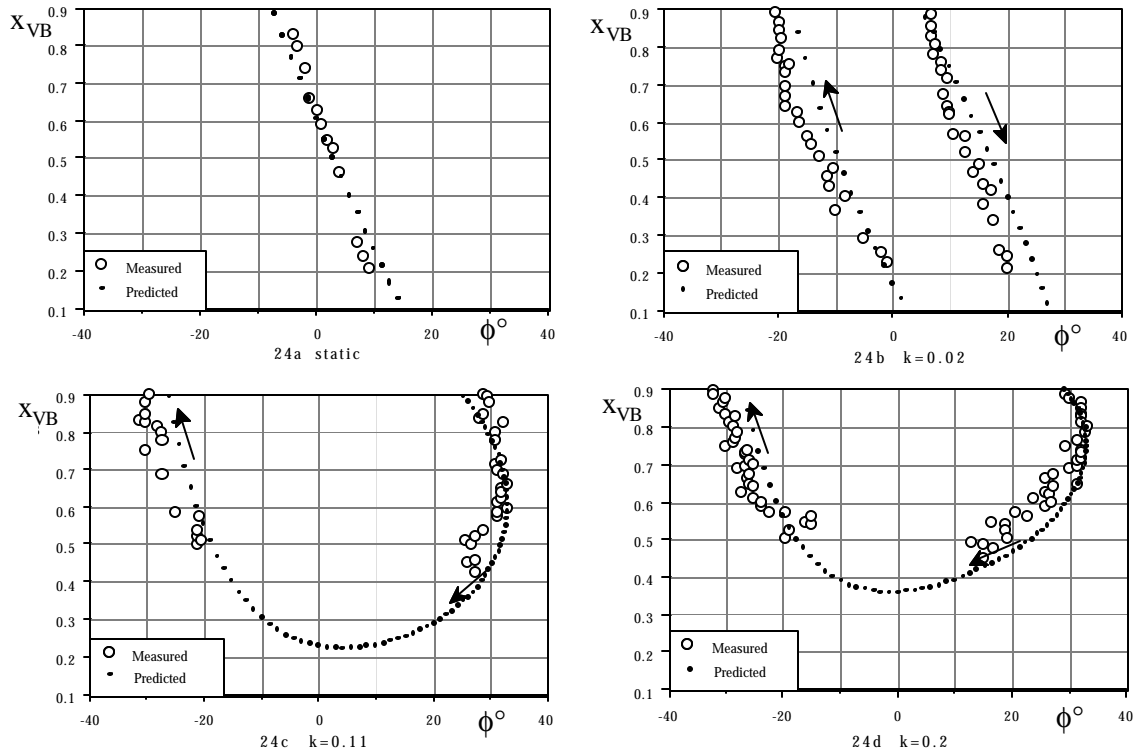Fig. 23 Vortex breakdown locations over flat wing and cambered wing halves (ϕ=0)

Fig. 24 Estimated and measured breakdown locations for rolled 65° delta wing (σ=30°)

Paper: 1
Author: Dr. Huang

<u>Question by Dr. Greenwell</u>: How was the vortex core size determined?

<u>Answer</u>: The vortex core diameter was determined by applying image analysis software to images of section view of the vortex ring. The gray level is proportional to the number of particles, which is the indication of vorticity strength. The location of maximum slope in gray level is approximately the edge of vortex core. Details can be found in my paper at the 8th ISFV.

<u>Comment, Dr. Greenwell</u>: See my later Paper 5: The radius of the smoke ring can be approximated as

$$r_{smoke} = \phi \, (d_p/3) \, \text{sqrt}[Re \, (\tau_p\text{-}1)]$$

Therefore, r_{smoke} is an indicator of the vortex swirl ratio, ϕ, and, therefore, is proportional to the vortex strength, Γ.

<u>Question by Prof. Slooff</u>: Has the prediction method been used for other configurations than the one(s) tested by the authors and, in particular, has it been applied to wings with a rounded leading edge?

<u>Answer</u>: We have used this method to predict delta wings with different sweep back angles in static conditions. A preliminary comparison has also been conducted for a 70° delta wing in dynamic (pitch) conditions. So far comparisons are only for sharp leading-edge delta wings. But in principle, this method can be applied to other shapes of leading edges for delta wings.

This page has been deliberately left blank

_____

Page intentionnellement blanche